Surface Ligands Increase Photoexcitation Relaxation Rates in CdSe Quantum Dots

Svetlana Kilina,[†,*] Kirill A. Velizhanin,[‡] Sergei Ivanov,[§] Oleg V. Prezhdo,[⊥] and Sergei Tretiak[¶,*]

[†]Department of Chemistry and Biochemistry, North Dakota State University, Fargo, North Dakota 58108, United States, [‡]Theoretical Division and Center for Nonlinear Studies, [§]MPA Division, Center for Integrated Nanotechnologies, and [¶]Theoretical Division and Center for Integrated Nanotechnologies, Los Alamos National Laboratory, Los Alamos, New Mexico 87545, United States, and [⊥]Department of Chemistry, University of Rochester, Rochester, New York 14627, United States

ABSTRACT

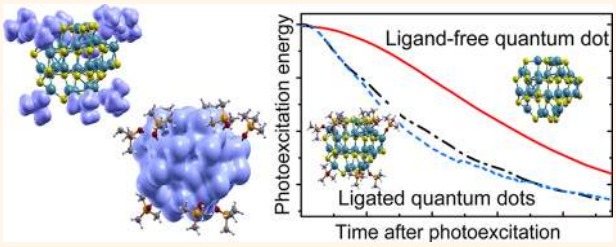

Understanding the pathways of hot exciton relaxation in photoexcited semiconductor nanocrystals, also called quantum dots (QDs), is of paramount importance in multiple energy, electronics and biological applications. An important nonradiative relaxation channel originates from the nonadiabatic (NA) coupling of electronic degrees of freedom to nuclear vibrations, which in QDs depend on the confinement effects and complicated surface chemistry. To elucidate the role of surface ligands in relaxation processes of nanocrystals, we study the dynamics of the NA exciton relaxation in $Cd_{33}Se_{33}$ semiconductor quantum dots passivated by either trimethylphosphine oxide or methylamine ligands using explicit time-dependent modeling. The large extent of hybridization between electronic states of quantum dot and ligand molecules is found to strongly facilitate exciton relaxation. Our computational results for the ligand contributions to the exciton relaxation and electronic energy-loss in small clusters are further extrapolated to larger quantum dots.

KEYWORDS: excitation relaxation · electron−phonon couplings · phonon-bottleneck · surface effects · nanocrystals

The energy of high energy photoexcitation ("hot exciton") in molecular and semiconductor materials is rapidly lost in the interband relaxation due to various mechanisms on femtosecond to picosecond time scale.[1] The most common nonradiative dissipation channel driving "electron cooling" is mediated by coupling to molecular vibrations and lattice phonons resulting in efficient conversion of an electronic energy into heat (so-called nonadiabatic relaxation). Such phonon-assisted energy relaxation is a key physical phenomenon and a limiting factor in many applications ranging from optoelectronics and photovoltaics to medicine. In this respect, colloidal semiconductor quantum dots (QDs) can be considered as very promising materials for the development of low cost and high efficiency devices, including lasing,[2,3] fluorescent biotagging,[4] quantum computing,[5] light-emitting diodes,[6] and solar cells.[7] In QDs, quantization of the electronic energy levels near the band edge induced by spatial confinement[8] results in a large energy splitting of electronic states and discrete atomic-like electronic transitions in contrast to continuous broad-band spectra of bulk semiconductors. Here, controlling and suppressing electron−phonon relaxation mechanisms may put forth other relaxation channels enabling several technological applications. For example, hot electron injection and carrier multiplication (CM) (or multiple exciton generation)[9] processes potentially allow for higher efficiency of QD-based solar cells. During CM several excitons are generated upon absorption of a single photon, which has been observed by femtosecond spectroscopy techniques in CdSe,[10] PbS and PbSe,[11] Si,[12] and InAs[13] QDs. Importantly, recent studies of PbS[14] and PbSe[15] quantum dots demonstrated collection of photocurrents with quantum yields greater than one electron per photon, thus confirming potential of CM for photovoltaic applications.[15] Singlet fission, a process similar to CM, was also shown to be very efficient in a number of molecular materials.[16]

In principle, in QDs with their well-separated electronic energies,[17] a large mismatch between the electronic and vibrational energy quanta promises a decrease in the electron−phonon relaxation, known as the phonon bottleneck.[8,9] However, time-resolved experiments have shown bulk-like

* Address correspondence to skilina@gmail.com, serg@lanl.gov.

Received for review May 29, 2012 and accepted June 28, 2012.

Published online June 28, 2012
10.1021/nn302371q

picosecond relaxation.[18−21] Moreover, the relaxation rates increase with decreasing QD size, even though the electronic energy spacing becomes larger.[22,23] Several origins of such fast energy relaxation in QDs have been suggested: (i) the Auger process, when the excited electron exchanges its energy with the coupled hole, and the hole then relaxes fast through its denser manifold of states[24−26] and (ii) surface process, including surface impurities, defects, and passivating ligands leading to intermediate states with strong electron−phonon couplings.[18,21,23,27] When both types of relaxation channels are suppressed, the energy relaxation time could be as long as 1 ns, revealing the phonon bottleneck.[28] This is achieved in QDs, where the emitting central core (CdSe) is surrounded by several shells of different thicknesses and compositions (CdS, ZnS, or ZnSe).[28] These shells protect the QD core from a surface environment and decouple electrons from holes, thus minimizing both relaxation mechanisms.[29,30]

Such materials where the shells well isolate photoexcitations, may not be suitable for applications, most notably, for photovoltaics, where electronic couplings between system components should be carefully engineered to achieve desired energy/charge transport. This frequently requires the use of a thin layer of specific surface ligands.[14,15] Consequently understanding and controlling mechanisms impacting relaxation rates are needed to rationally design materials for specific applications. Experimentally, only intraband relaxation rates of relatively low-lying excited states (near the QD's band gap) have been studied in detail.[22,23,28] However, the mechanisms of fast photoexcited carrier relaxation in the region of higher excitation energies (at three times of the band gap)—being extremely important for CM and other processes—are still under debate. In experiment, it is very challenging, if not impossible, to separate contributions of ligands, surface defects, and Auger recombination to the intraband relaxation.

Consequently, the current conclusion from the experimental data is of qualitative nature: ligands do affect (enhance) relaxation of hot carriers in semiconductor quantum dots. Reports[19,23,27,31,32] have shown that the hole relaxation even for low-lying states (*i.e.*, near band edge) is dominated by the ligand-mediated nonadiabatic channel. Here, the hot electron relaxation (again near the band edge) was not strongly affected by ligands, because the dominating channel was the Auger-type relaxation, where an electron efficiently transfers energy to the hole. In other experiments, where this Auger channel was suppressed,[27] the hot electron relaxation was unambiguously demonstrated to be affected by the presence of ligands. More quantitative and specific aspects of the ligand contribution to the relaxation rates are required − in particular, why does it happen, how does it happen, and at which excitation energies do ligands affect the relaxation processes. Theoretical simulations at the atomistic level are expected to provide answers to those questions. However, despite a large body of work, a theoretical description of nonadiabatic relaxation channels induced by surface and ligand's states is limited. The challenge originates from uncertainty of the chemical compositions and surface morphologies owning very complicated chemistry of QD−ligand interfaces. Current theoretical work mainly focuses on characterization of QD structure[33−38] and spectra[39−48] with a few efforts devoted to direct real-time dynamical simulations[49,50] and models[51] of experiments that probe charge−phonon dynamics in QDs. On the other hand, well-developed theories already exist for the Auger-relaxation mechanism,[24,52,53] as well as for impact ionization rates in QDs[54,55] to describe the CM process. However, to obtain the efficiency of CM, accurately calculated rates of impact ionization are universally multiplied by some approximate constant (an average intraband relaxation time) essentially annihilating all the accuracy gained. As such, quantum-chemical calculations providing energy-resolved relaxation rates in QDs are needed. To cover the existing gap in theoretical descriptions of photoexcited dynamics in QDs, we provide our investigations of pure nonadiabatic relaxation mechanisms and, specifically, of the role of surface ligands in these processes.

Here, our direct modeling of nonadiabatic (NA) intraband photoexcitation dynamics in the ligated CdSe QD provides detailed theoretical description of the electron−phonon relaxation channel at the atomistic level. Using the time-dependent Kohn−Sham (TDKS) approach,[56] we study photoexcitation dynamics up to 1 ps in a $Cd_{33}Se_{33}$ cluster passivated by commonly used ligands, phosphine oxides ($OPMe_3$) and primary amines (NH_2Me), as well as the ligand-free system. We show that ligands introduce a specific manifold of high-energy hybridized electronic states, where the electronic density spreads over the QD surface and ligand atoms. Such states feature strong electron−phonon couplings to both high frequency vibrations of the ligand atoms and low-frequency surface phonons, thus facilitating fast intraband electron−hole (e−h) relaxation. Consequently, our simulations reveal that at the excitation energies larger than 2.5 times of the QD's energy gap, hybridized orbitals significantly impact the relaxation rates; that is, the intraband photoexcitation relaxation occurs up to twice as fast in ligated QDs as in the ligand-free (bare) cluster. Calculated relaxation rates are further extrapolated to different CdSe QD sizes.

RESULTS AND DISCUSSION

We start our modeling with constructing three systems, $Cd_{33}Se_{33}$, $Cd_{33}Se_{33}$+9$OPMe_3$, and $Cd_{33}Se_{33}$+9NH_2Me clusters (see Figure 1a). The ligands were

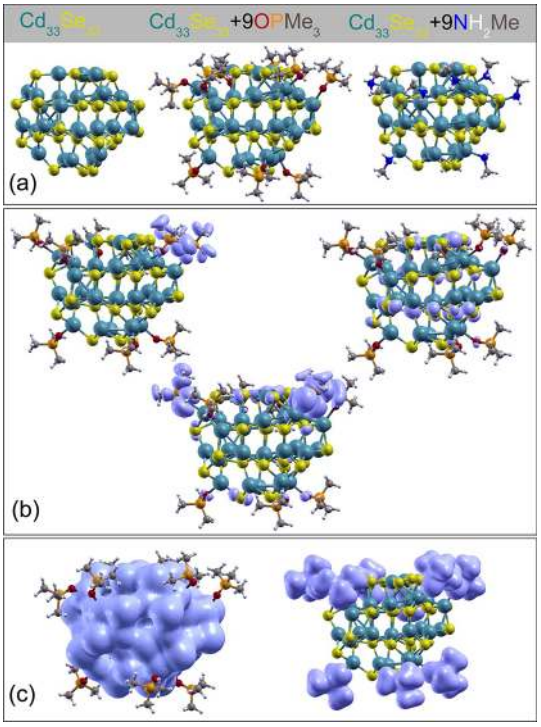

Figure 1. (a) Structures of the bare and ligated $Cd_{33}Se_{33}$ clusters studied here. Shown snapshots are taken at 250 fs of the respective MD trajectories at room temperature. (b) Partial charge densities ($\rho_n = |\psi_n(r)|^2$) representing typical KS states localized on ligands, on the QD, and delocalized over the QD and ligands (hybridized state) of the $Cd_{33}Se_{33}$+9OPMe$_3$ cluster. (c) The isosurfaces of the QD (left) and ligand layer (right) defined by eqs 3 and 4 used to calculate the fragment decomposition of the DOS in Figure 2.

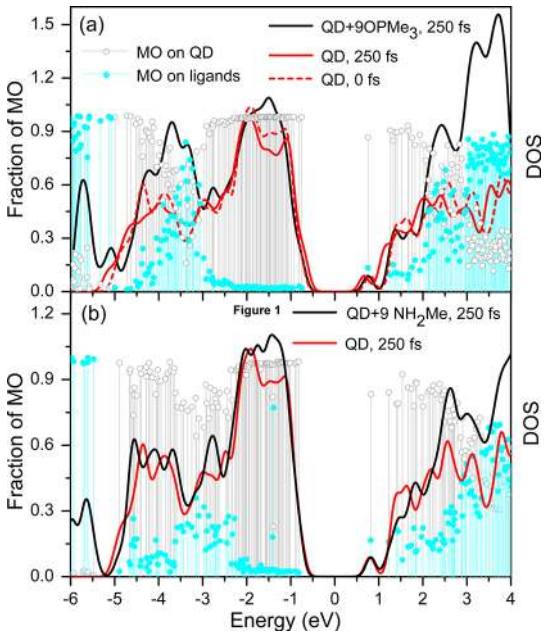

Figure 2. The density of states (DOS) and its fragment analysis providing portions of the MO density localized at the QD (vertical gray sticks) and ligands (vertical cyan sticks). The solid lines correspond to the DOS of the bare $Cd_{33}Se_{33}$ (red lines in panels a and b), $Cd_{33}Se_{33}$+9OPMe$_3$ (black line in panel a) and $Cd_{33}Se_{33}$+9NH$_2$Me (black line in panel b) clusters. Calculations are done using geometries taken at 250 fs of the respective MD trajectories at room temperature (solid lines) and optimal geometry of the bare QD (dashed red line in panel a). The Fermi energy is chosen to be in the middle of the HOMO−LUMO gap. The orbitals near the band gap primarily have the QD-localized character, while apart from the band gap, orbitals are hybridized between QD and ligands.

attached to the most chemically active surface atoms (all 2-coordinated Cd atoms on the cluster surface) as described the previous studies.[41] Recent experiments[57] have shown that such small "magic"-size QDs with diameters smaller than ~2 nm demonstrate great stability, the controllable size and shape, and reproducible optical properties, including a strong blue-light emission. The $Cd_{33}Se_{33}$ "magic" structure with diameter of 1.3 nm has been experimentally shown to be very stable,[58] while it is the smallest cluster that supports a crystalline-like core.[34,41] This makes the $Cd_{33}Se_{33}$ cluster an excellent model for quantum-chemical studies of electronic properties of CdSe QDs. Even passivated with multiple ligands, the system requires reasonable computational efforts for atomistic modeling based on Density Functional Theory (DFT). Our three molecular systems have been optimized and further equilibrated at 300 K providing an input for NA dynamics calculations as described in the section Computational Methodology. As shown in Figure 1a, the obtained geometries at room temperatures deviate from the initial bulk configuration, although the rough bulk-like structure is recognizable. Surface reconstruction is similar in both ligand-free and passivated QDs: Significant surface reconstruction occurs even in the presence of ligands passivating the QD's surface. These results well correlate with X-ray photoelectron spectroscopy measurements of CdSe[59] and PbSe[60] QDs, revealing distinct morphologies of the inner (core) and outer (surface and surface-ligand) QD's atoms. The surface reconstruction results in the saturation of unsaturated valencies and removal of associated localized surface states (self-healing).[34] Consequently, this opens the energy gap (here the gap between the highest occupied (HOMO) and lowest unoccupied (LUMO) Kohn−Sham molecular orbitals) of CdSe clusters, which is well studied in the previous DFT calculations.[34,41]

As expected, all considered clusters have pronounced energy gaps of ~1.6 to 1.8 eV (see Figure 2). These values are underestimated, a typical feature of all semilocal DFT functionals such as PW91 used in our calculations. Correcting the functional with a small portion of orbital exchange (*e.g.*, B3LYP hybrid model), leads to an increase of the energy gap in the same structures (~3 eV),[41] which agrees well with the lowest absorption peak (~3 eV) experimentally observed and assigned to the $Cd_{33}Se_{33}$ QD.[58,61] Except for the energy gap, change of the DFT model insignificantly affects the QD's electronic structure and the density of states (DOS).[41]

Figure 2 compares the DOS calculated using eq 1 for the bare and ligated $Cd_{33}Se_{33}$ QDs at room temperature. The energy levels have been computed along a 1 ps molecular dynamics (MD) trajectory. For comparison, Figure 2 shows the DOS of the ligand-free cluster at the initial moment of MD and random snapshots of both bare and ligated QDs at 250 fs. The time evolution along the MD trajectory at 300 K for all systems results in small fluctuations of the DOS while the overall electronic structure is preserved. The DOS of the bare and ligated clusters is roughly the same near the edge of the energy gap. Inside the bands, however, the DOS of the ligated clusters reveals a lot of additional states resulting in more intense peaks due to passivation. To understand the character of these additional states, we further analyze the spatial distribution of the molecular orbitals (MOs). For each electronic state of the passivated QDs, we calculate the fraction of the Kohn–Sham (KS) wave function norm $|\psi_i(\mathbf{r})|^2$ (partial charge density) that resides in the region of the QD and in a shell around the surface-ligand, as determined by eqs 3 and 4 and illustrated in Figure 1c. Figure 2 shows that states near the band gap have partial charge density mostly localized on the QD, thus, explaining why the DOS of the bare and ligated QDs nearly coincide in this region. In the energy regions where the DOS of the bare QD significantly deviates from the DOS of the passivated clusters, many of the MOs are hybridized spreading over both QD and ligand atoms. Notably, energies of such new bands associated with hybridized states vary for different ligands (Figure 2). Consequently, photoexcitation energy relaxation rates in the passivated QD are expected to be dependent on the chemical composition of capping ligands. Figure 1b illustrates three different types of states found in the DOS of capped QDs, that is, states localized on the QD, ligand molecules, and surface atoms being hybridized between QD and ligands. Our results obtained from the MD simulations agree well with previous DFT calculations of the electronic structure of these clusters at equilibrium[41] and recent pseudopotential modeling.[62]

Even though most of the hybridized states are not optically active,[41] their presence cannot be ignored during photoexcitation dynamics. Figure 3a shows calculated absorption spectra of the bare and passivated $Cd_{33}Se_{33}$. These are computed using eqs 1–2 on the basis of a single particle approximation, when the transition energy is the difference between energies of the electron and hole states ($\varepsilon_l - \varepsilon_k$). The distribution of the energies and oscillator strengths for electron–hole pairs of each QD in the ensemble allows us to construct a realistic initial photoexcited state in a form of the wavepacket for subsequent NA dynamics simulations, as described in the Computational Methodology section.

The energy of an excited electron can be further defined with respect to the energy of LUMO ($E_e = \varepsilon_l - E_{LUMO}$) and

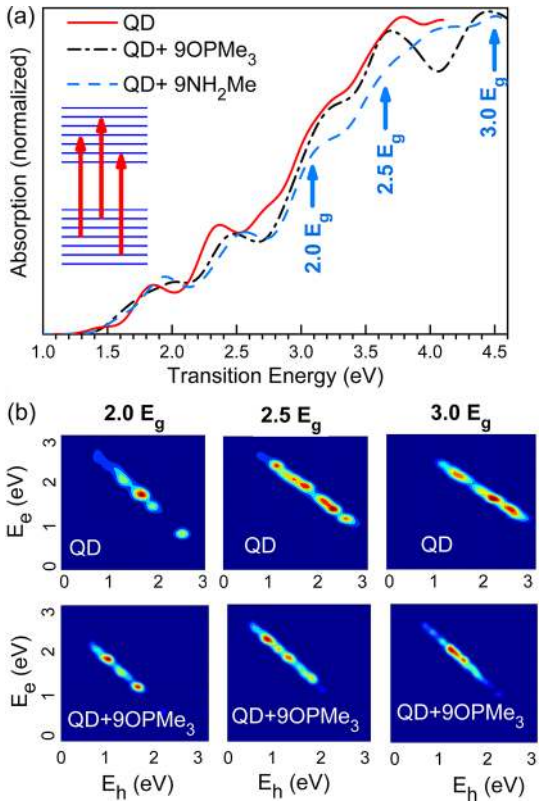

Figure 3. (a) Calculated absorption spectra of the bare and ligated $Cd_{33}Se_{33}$ clusters averaged over 250 configurations for each system taken along the respective 1 ps MD trajectories at room temperature. The arrows show the centers of the initial photoexcited wavepackets at 2, 2.5, and 3 times the band gaps used for NA MD simulations. The inset illustrates symmetric and asymmetric e–h transitions that contribute to the optical spectra. (b) Two-dimensional representation of optical absorption as a function of photoexcited electron and hole energies calculated for the bare $Cd_{33}Se_{33}$ (top) and $Cd_{33}Se_{33}$+9OPMe$_3$ (bottom) clusters. *X* and *Y* axes span energies of hole and electron states, respectively, while optical intensity (oscillator strength) of every possible transition is defined by a color in a rainbow manner from red to blue. The total excitation energy of the e–h pair is fixed at 2, 2.5, and 3 times the respective band gaps (columns).

the energy of a hole with respect to the HOMO ($E_h = E_{HOMO} - \varepsilon_k$). Note that both symmetric ($E_e \approx E_h$) and asymmetric ($E_e > E_h$ or $E_e < E_h$) excitations might potentially contribute to the optical absorption (inset in Figure 3a) depending on the excitation energy (*e.g.*, arrows in Figure 3a). Two-dimensional plots in Figure 3b analyze relative contributions of such symmetric and asymmetric transitions to the absorption spectra. These plots demonstrate that for any energy, the overall photoexcited wavepacket is given by a complex combination of symmetric and asymmetric transitions. The dominant character of asymmetric transitions assumes that either an electron or a hole can be excited to the range of the DOS where hybridized states are present. For example, for excitation at about 2.5 times of the energy gap ($2.5E_g$) with the dominant contribution of asymmetric transition $E_e > E_h$, the hole is excited in the

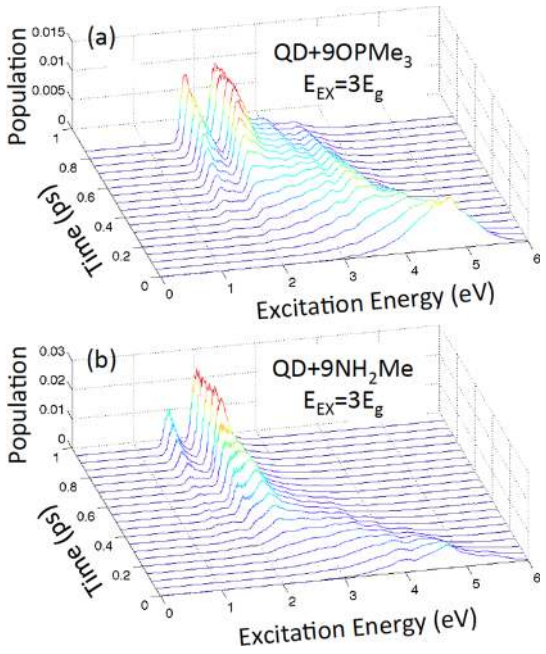

Figure 4. Time evolution of the photoexcited wavepacket in $Cd_{33}Se_{33}$+9OPMe$_3$ (a) and $Cd_{33}Se_{33}$+9NH$_2$Me (b) clusters. The initial excitation energy corresponds to 3 times the energy gap.

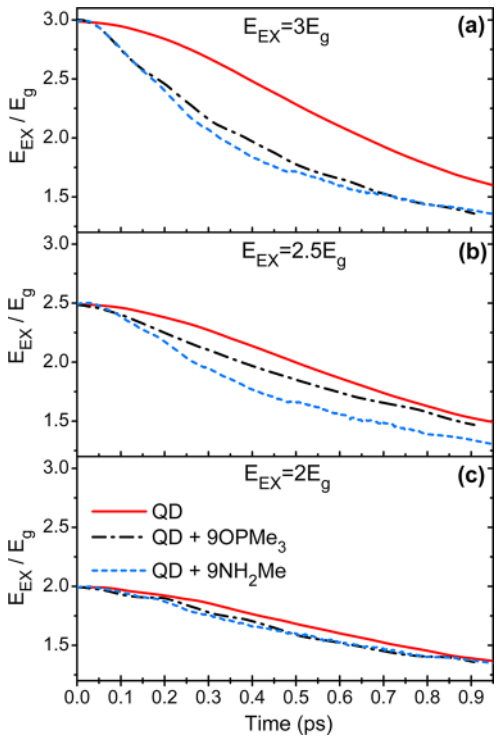

Figure 5. Time evolution of the averaged energy of the photoexcited wavepacket in the ligand-free and ligated QDs after initial excitation at 3 (a), 2.5 (b), and 2 (c) times of the band gap.

range where most of orbitals are localized on the QD, while the electron appears at energy where the DOS is prevailed by the hybridized states (Figure 2). Note that for the ligated QDs, photoexcitations with energies higher than $2.5E_g$ have mostly asymmetric character with the higher energy of electrons than holes, thus, providing significant contribution of hybridized electronic states to photoexcited dynamics.

We next discuss our NA dynamics simulations constituting the main result of this study. Time evolution of the photoexcited wavepacket with initial excitation energy of about 3 times the energy gap for passivated $Cd_{33}Se_{33}$ clusters is shown in Figure 4. Here, the wavepacket is a histogram of the DOS of excited e−h pairs with a given energy at each moment of time during NA dynamics. Variation of this quantity as a function of energy and time represents relaxation of the photoexcitation mediated by coupling to phonons. The nonequilibrium wavepackets in both cases (Figure 4) are initially broadened by a chosen line width (0.6 eV), spread even further due to significant density of e−h pairs at high excitation energies, and finally reappear as two sharp peaks close to the energy gap. The multipeak structure of the wavepacket after ~1 ps dynamics reflects large energy splitting (~0.5 eV) between the LUMO and LUMO+1. Overall, the main part of the relaxation is completed within a picosecond, which agrees with experimental measurements in passivated CdSe QDs.[18−21]

Following the example described above, for all three QDs we performed 1 ps NA dynamics simulations starting from the different initial photoexcitation energies, namely excitations at $2E_g$, $2.5E_g$, and $3E_g$ (marked by arrows in Figure 3a). The resulting relaxation of the average energy of the photoexcited e−h pairs is compared in Figure 5. This figure represents the time-dependent average energy of a wavepacket (approximately the maximum of the wavepacket at each moment of time) and is obtained from Figure 4 by averaging the energy of the wavepacket at each time step. For the lowest energy excitation at $2E_g$, relaxation dynamics is very similar in all three clusters (Figure 5c). This is expected, since the low-energy excitations involve e−h pairs from the energy range where the DOS of the bare and passivated QDs is similar, and all orbitals are localized on the QD (see Figure 2). For excitation energies greater than $2.5E_g$, relaxation occurs noticeably faster in the ligated QDs (Figure 5b,c). Such fast relaxation in the passivated clusters originates from the strong electron−phonon couplings provided by dense hybridized states. Even if an electron or a hole is not initially excited to the hybridized orbital, NA coupling between electronic states forces the charge to jump to one of the neighboring hybridized states, which is coupled to both high-frequency vibrations of the ligands, and low-frequency surface, acoustic, and optical phonons of the cluster, thus opening new channels for electron−phonon relaxation.

The difference in the relaxation time between amine and phosphine oxide ligated QDs for $2.5E_g$ case

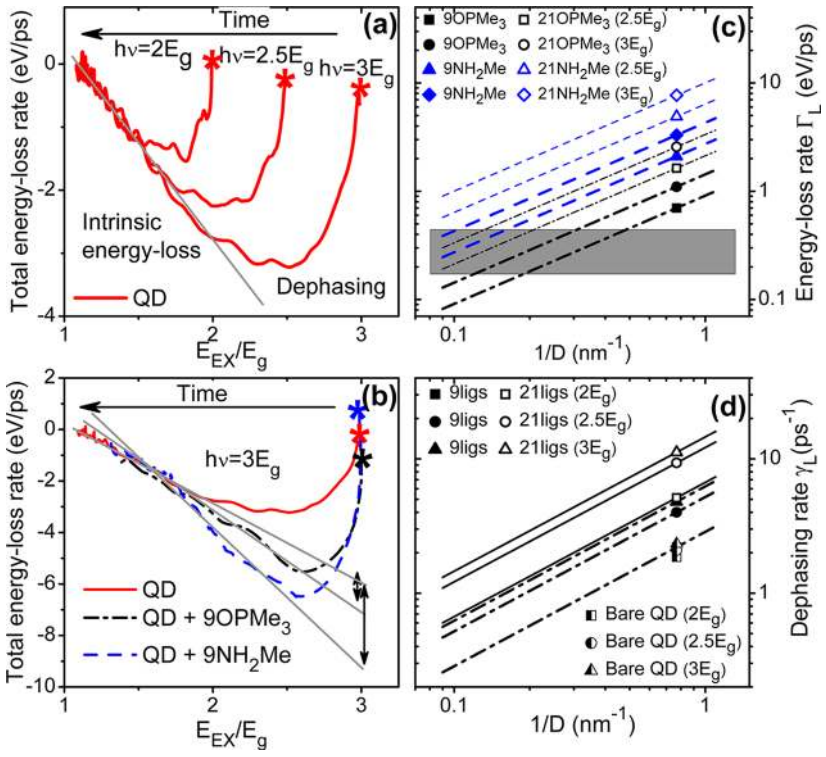

Figure 6. (a) Calculated exciton energy-loss rates in the ligand-free $Cd_{33}Se_{33}$ cluster at various initial photoexcitation energies. (b) Energy-loss rate in the ligand-free and ligated QDs calculated for the initial photoexcitation energy of $3E_g$. Starting points of the dynamics are marked by the "star" symbols. Double-sided arrows show the ligand layer contribution to the linearly fitted intrinsic energy-loss rates in ligated QDs. (c) The size-extrapolated ligand contribution to the exciton energy-loss rates for low (thick lines) and high (thin lines) ligand densities. The low (1.7 ligands/nm^2) and high (4 ligands/nm^2) ligand densities correspond to $Cd_{33}Se_{33}$ passivated with 9 and 21 ligands, respectively. The filled symbols show the ligand contribution to the energy-loss rate Γ_L at different initial photoexcitation energy for $Cd_{33}Se_{33}$ cluster passivated with nine ligands, as extracted from panel b. The corresponding empty symbols display the same quantities but extrapolated for high ligand density ($Cd_{33}Se_{33}$ passivated with 21 ligands). The gray bar outlines the range of energy-loss rates in the bulk CdSe material. (d) The size-extrapolated ligand contribution to the dephasing rates γ_L for low (dashed lines) and high (solid lines) ligand densities. The filled and empty symbols show the dephasing rates obtained from Figure 5 for the ligated $Cd_{33}Se_{33}$ cluster, which are weakly dependent on the ligand nature. For comparison, calculated dephasing rates for ligand-free $Cd_{33}Se_{33}$ QDs are shown by the half-filled symbols.

(Figure 5b) further emphasizes an importance of hybridized states. The QD ligated with NH_2Me exhibits the fastest relaxation, while the relaxation rate in the $OPMe_3$ ligated QD is only slightly increased compared to the bare cluster. This occurs because the hybridized states of holes in the valence band of the QD+$9NH_2Me$ cluster are located closer to the energy gap compared to that of QD+$9OPMe_3$ cluster (see Figure 2). At the highest excitation energy $3E_g$, hybridized states in both valence and conduction bands can equally contribute to electron−phonon couplings in both ligated QDs and, consequently, the relaxation rates are nearly the same in both clusters (Figure 5a). Notable, the relaxation rate is strongly dependent not only on the energy of photoexcitation, but also on the nature of the initial wavepacket in term of "symmetric" and "asymmetric" e−h pairs (see Figure 3 and Figure 1S in Supporting Information). Overall we observe that the initial photoexcitation at $3.0E_g$ (*i.e.*, near the experimentally observed threshold energy for CM)[10] in the ligated QDs relaxes almost two times faster compared to that of the bare cluster.

It is important to emphasize that the higher DOS of the ligated QDs is not the sole factor that speeds up the relaxation. For example, states with energies at ~1.5 eV from the edges of the energy gap contribute to the excitations at $2.5E_g$ (compare panels a and b in Figure 2). The DOS at such energies of the amine- and phospine oxides-ligated QDs is similar and much larger compared to the bare cluster. Nonetheless, the relaxation rate is faster in amine-ligated QDs compared to that of $OPMe_3$-ligated QDs at $2.5E_g$ excitation energy (Figure 5b). States with energies at 2−2.5 eV from the edges of the energy gap contribute to excitations at $3E_g$. Here the DOS of the phospine oxides-ligated QD is significantly higher than the DOS of the amine-ligated QD, while the relaxation rate is slightly faster in amine-ligated clusters (Figure 5c). These results point out that the carrier relaxation rates are controlled by specific electron−phonon couplings present in ligand molecules, rather than just increased DOS due to hybridized states.

To analyze the exciton relaxation dynamics, we represent the total energy-loss rate as a function of

energy in Figure 6a,b. These energy-loss rates are obtained as the dependence of time derivative of the exciton energy on the instantaneous exciton energy of the bare and ligated QDs, normalized by the energy gap of the system. As can be seen in Figure 5 showing the time-dependence of exciton energies, the exciton relaxation is hindered immediately after photoexcitation, demonstrating a weak time dependence of the exciton energy at $t \lesssim 0.1$ ps. This slow relaxation reveals itself in Figure 6a,b as a vanishing energy-loss rate at exciton energies close to the corresponding energies of photoexcitation. This vanishing energy-loss rate at $t = 0$ was previously argued to be a manifestation of the quantum Zeno effect.[63] At $t > 0$, the electron−phonon interaction results in dynamical *decorrelation* between the phases of electronic wave functions of different QDs within the statistical ensemble (*dephasing* process). This dephasing leads to a mixed (*nonpure*) electronic state of the system resulting in a nonvanishing energy-loss rate. Once dephasing is completed, the energy-loss rates vary almost linearly with energy, as highlighted by the linear fitting shown as the gray lines in Figure 6a,b.

Subsequently, we separate the dephasing contribution (complicated initial relaxation stage) from the *intrinsic* incoherent energy-loss process (linear dependence of the energy-loss rates on the exciton energy at later times), as marked in Figure 6a,b. Taking into account only the *intrinsic* energy-loss, the energy-loss rates can be approximated as a slope of the linear fitting shown by gray lines in Figure 6a,b. For example, the intrinsic energy-loss rate for the bare QD at $3E_g$ is about −6 eV/ps. The dephasing time is then approximately defined by a position of the inflection point of a corresponding plot in Figure 5. Obtained pure energy-loss rates and dephasing times for all systems we considered are summarized in Tables 1 and 2 of Supporting Information. For the ligated QDs the dephasing times are about two to three times faster than those of the bare QD. The pure energy-loss rates are also faster in the ligated QDs.

As shown in Figure 6b, comparison of the *intrinsic* energy-loss rates of QDs photoexcited at $3E_g$ demonstrates that at energies less than $1.5E_g$, the effect of ligands on the energy-loss dynamics is minor resulting in a very similar behavior of bare and ligated QDs. However, energy-loss rates are increased at higher energies in ligated QDs. The difference in respective slopes quantifies the contribution of ligands to the pure energy-loss rates, see Table 2 in the Supporting Information. Owing to high numerical cost, our atomistic TDKS simulations allow to model NA dynamics only in small QDs and a few cases. We further extrapolate obtained results on the ligand role in the photoinduced dynamics to different surface density of ligands and different QDs sizes. We define the ligand contribution to the intrinsic energy-loss rate Γ_L, as a difference between energy-loss rates for QDs with and without ligands. At a constant surface density of ligands, Γ_L is expected to be inversely proportional to the QD diameter D. Indeed, the probability of a carrier to be near the surface of QD, and, therefore, undergo the ligand-mediated relaxation, is proportional to $S/V \sim 1/D$, where $S \sim D^2$ and $V \sim D^3$ are the surface area and the volume of QD, respectively. Furthermore, if the QD size remained the same, Γ_L should be proportional to the surface density of ligands σ. These scaling relations can be combined into a single expression $\Gamma_L = \Gamma_{L,0}(\sigma/\sigma_0)(D/D_0)^{-1}$ where $\Gamma_{L,0}$, σ_0, and D_0 are the ligand contribution to the exciton energy-loss rate, the surface density of ligands, and the diameter of the $Cd_{33}Se_{33}$ cluster studied by the TDKS approach. The surface density of ligands for $Cd_{33}Se_{33}$, σ_0, corresponds to either the NH_2Me or the $OPMe_3$ ligand shell.

Figure 6c shows the expected behavior of Γ_L with the QD diameter (1−10 nm) and the low (σ_0 = 1.7 ligands/nm^2) and high (σ_0 = 4 ligands/nm^2) ligand densities calculated using the scaling relation obtained above. For comparison, the gray bar in Figure 6 represents the range of energy-loss rates obtained from the Fröhlich model of carrier relaxation in bulk CdSe at excitation energies between 4.8 and 3.2 eV, which correspond to $3E_g$ and $2E_g$ cases for $Cd_{33}Se_{33}$, respectively. Note that at the initial excitation energy of $2.5E_g$ the ligand contribution to the energy-loss rate dominates the relaxation dynamics only for the smallest QDs ($D < 2$ nm). At the higher excitation energy ($\sim 3E_g$), the ligand contribution is substantial over the entire range of QD sizes considered. The same scaling analysis applied to the ligand contribution to the dephasing rate, similarly shows significant ligand role at the higher excitation energies ($\geq 3E_g$) (see Figure 6d). We note that low dephasing rates allow another relaxation mechanism (for example, CM[14,15]) to take place right after photoexcitation without significant heat losses.

CONCLUSIONS

Experimental studies of the hot carrier relaxation for low-laying excited states[18,21,23,27,31] have shown that it is extremely dependent on the QD size/shape. Investigations of the region of higher excitation energies ($>2.5E_g$), which is very important for many promising phenomena (*e.g.*, CM), is experimentally challenging. Here we employ the TDKS theory[56] to model nonadiabatic photoexcitation dynamics in small QDs passivated by commonly used ligands. Our results provide detailed theoretical description of ultrafast phonon-assisted relaxation of excited e−h pairs, explain at the atomistic level mechanisms of this dynamics, and determine the role of surface ligands in this process. We have found that at the excitation energies larger than 2.5 times the QD's energy gap, surface ligands significantly increase electron−phonon mediated relaxation rates compared ligand-free small CdSe QD

clusters. At such excitation energies the ligands introduce to the electronic structure of the CdSe QD new manifold-hybridized orbitals delocalized over surface QD atoms and ligand molecules. Such hybridized orbitals are characterized by increased electron−phonon couplings to the high frequency vibrations of the ligands, thus opening new relaxation channels allowing for ultrafast photoexcitation relaxation rates which are typical for small molecules. Extrapolation of our computational results to different QD sizes and ligand densities suggests that for commonly used in experiment CdSe nanocrystals with 4−7 nm diameters, surface ligands can significantly affect phonon-assisted relaxation rates at high photoexcitation energies, which may become a competing mechanism to other relaxation processes (CM[14,15]). Thus, our computational work provides theoreticians with energy-resolved relaxation rates across the broad excitation region, clarifies the effect of ligands (including the dependence on excitation energy) on intraband carrier relaxation, and intends to stimulate experimental efforts in measuring the intraband relaxation rates in the high energy domain.

COMPUTATIONAL METHODOLOGY

We apply time-domain Kohn−Sham (TDKS) method[56] to computationally model phonon-assisted dynamics of electrons and holes in $Cd_{33}Se_{33}$ passivated by $OPMe_3$ and NH_2Me ligands. Each studied cluster is initially constructed from a wurtzite lattice with bulk Cd−Se bond lengths and then is relaxed to its lowest energy configuration (see Figure 1). The geometry optimization procedure is performed using DFT with a plane wave basis set, as incorporated in the VASP code.[64] The Generalized Gradient Approximation (GGA) functional of Perdew and Wang (PW91)[65] coupled with the Vanderbilt pseudopotentials[66] was used for all electronic structure computations. The simulations are carried out in a cubic cell periodically replicated in three dimensions, as stipulated by the plane wave basis. To prevent spurious interactions between periodic images of the QD, each cell was constructed to have at least 8 Å of vacuum between the QD replicas.

To model vibrational dynamics, the optimized QD structures are heated to 300 K by repeated velocity rescaling, as implemented in the VASP software. A microcanonical MD trajectory of 1.2 ps long has been then generated for each cluster in the ground electronic state using 1 fs nuclear and 10^{-3} fs electronic time-steps. From this trajectory, 250 random initial configurations are sampled to create an ensemble of QDs. The obtained trajectories of each QD from the thermodynamic ensemble have been further used to perform simulations of the electron−phonon relaxation dynamics based on the implementation of the fewest switching surface hopping (FSSH) technique[67,68] into the TDKS scheme within the VASP software[49,56] (see Supporting Information). The FSSH is a nonadiabatic molecular dynamics methodology which uses a stochastic algorithm that generates trajectory branching[67] and satisfies detailed balance.[68] This approach is currently broadly used to study relaxation processes and decay to thermodynamic equilibrium in a variety of molecular materials.[69−71]

For the FSSH technique, the initial electronic state has to be defined. For this, we construct initial photoexcited states based on the distribution of energies and oscillator strengths for electron−hole pairs of QDs in the ensemble (see details in Supporting Information). At initial moment of time, for each QD in the ensemble, a single pair of KS orbitals (one from the valence and one from the conduction bands) is chosen so that (i) they form an electron−hole pair of the energy no farther than ±0.3 eV from the specified excitation energy (*e.g.*, two or three times the energy gap of the QD), and (ii) this pair gives the highest oscillator strength within this energy range. The initial energy of the electron−hole pair of each QD from the ensemble forms a finite-width distribution in the energy domain, which allows us to construct a realistic initial photoexcited state in a form of the wavepacket. This wavepacket undergoes time evolution during subsequent NA dynamics simulations, as illustrated in Figure 4.

The density of states (DOS) and optical absorption spectra of QDs are calculated within a single-particle KS orbital representation using the Gaussian line-broadening:

$$A(\omega) = \frac{1}{\sigma\sqrt{\pi}}\sum_n h_n \exp\frac{-(\omega_n - \omega)^2}{\sigma^2} \quad (1)$$

where ω_n is the transition energy, h_n is the oscillator strength, and σ is an empirical line-broadening parameter. For DOS calculations shown in Figure 2, $\omega_n = \varepsilon_n$ (ε_n being the nth KS orbital energy, and the index n runs over occupied and virtual states), $h_n = 1$ and $\sigma = 80$ meV. For absorption spectra calculations shown in Figure 3, $\omega_n \equiv \omega_{kl} = \varepsilon_k - \varepsilon_l$ (ε_k and ε_l being the energies of the virtual and occupied orbitals, respectively, and the indices k and l run over the occupied and virtual orbital space, respectively), and $h_n \equiv h_{kl} = f_{kl}$ is the oscillator strength of the respective transition between kth (an electron) and lth (a hole) KS states defined as

$$f_{kl} = \frac{2m_e(\varepsilon_k - \varepsilon_l)}{3\hbar^2}\mu_{kl}^2 \quad (2)$$

where $\mu_{kl} = \langle\psi_k|\hat{\mu}|\psi_l\rangle$ is the transition dipole moment, ψ_k and ψ_l are the respective KS wave functions, m_e is an electron mass, and $\hat{\mu}$ is the dipole moment operator. For calculations of optical spectra, the chosen line width $\sigma = 30$ meV is comparable to experimental inhomogeneous spectral broadening.

The fraction of the KS wave function norm $|\psi_n(\mathbf{r})|^2$ (partial charge density) that resides in the region of the QD (gray vertical lines in Figure 2) is calculated as

$$F_n = \int_{\mathbf{r}\in S}|\psi_n(\mathbf{r})|^2 \quad (3)$$

Here S is the shell around the surface Cd and Se atoms that we define by comparing the magnitude of the total electronic density (r) of the ligated QD when ligands are removed, to a specific tolerance parameter ε at each grid point r of the simulation cell:

$$S(r) = \begin{pmatrix} 0, & \overline{\rho}_n(r) < \varepsilon \\ 1, & \overline{\rho}_n(r) \geq \varepsilon. \end{pmatrix} \quad (4)$$

The tolerance parameter ε characterizes the radius of the isosurface for a ligand-free QD, as illustrated in Figure 1c. Analogously, we compute the fraction of the partial charge density localized on ligands. Here S is constructed from the total charge density of the ligated QD with removed QD part (Figure 1c).

The range of exciton energy-loss rates in bulk CdSe at excitation energies between 3.2 and 4.8 eV (gray bar in Figure 6c) is estimated from the Fröhlich model of carrier relaxation in bulk semiconductor materials. Specifically, we calculate the electron energy-loss rate by using the Fröhlich expression[72]

$$\frac{dE}{dt} = \beta\hbar\omega_0^2\left(\frac{\hbar\omega_0}{E}\right)^{1/2}\ln\left(\frac{4E}{\hbar\omega_0}\right) \quad (5)$$

where $\beta = 0.46$ is the polar-interaction constant in CdSe. The optical phonon energy in bulk CdSe is $\hbar\omega_0 \approx 25$ meV. Using the formula for *electron* energy-loss rate we then evaluate the *exciton* energy-loss rate assuming that all the excitation energy is absorbed by the electron and a hole kinetic energy is negligible. This approximation is fairly accurate for bulk material given large difference of the hole and electron effective masses in CdSe.[73]

Conflict of Interest: The authors declare no competing financial interest.

Acknowledgment. The authors wish to thank Victor I. Klimov, Andrei Piryatinski, and Dmitri Kilin for fruitful discussions and comments. S.T. and K.A.V. acknowledge support from the Center for Advanced Solar Photophysics, an Energy Frontier Research Center funded by the U.S. Department of Energy (DOE), Office of Science, Office of Basic Energy Sciences (BES). S.K. acknowledges financial support from NDSU Advance FORWARD program sponsored by NSF HRD-0811239 and ND EPSCoR through NSF Grant No. EPS-0814442 for providing renovated lab space and DOE Grant No. DE-FG36-08GO88160 dedicated to the solar cell studies. O.V.P. acknowledges financial support of DOE, Grant No. DEFG02-05ER15755, dedicated to the QD studies, and NSF, Grant No. CHE-1050405, supporting methods development. The work has been conducted in part at the Center for Integrated Nanotechnologies at Los Alamos National Laboratory (LANL). We also acknowledge support provided by the Center for Nonlinear Studies (LANL). LANL is operated by Los Alamos National Security, LLC, for the National Nuclear Security Administration of the U.S. DOE under contract DE-AC52-06NA25396.

Supporting Information Available: Description of the Time-Domain Kohn−Sham (TDKS) computational methodology and calculated exciton energy loss rates. Two videos. This material is available free of charge *via* the Internet at http://pubs.acs.org.

REFERENCES AND NOTES

1. Frolov, S. V; Bao, Z; Wohlgenannt, M; Vardeny, Z. V. Ultrafast Spectroscopy of Even-Parity States in Pi-Conjugated Polymers. *Phys. Rev. Lett.* **2000**, *85*, 2196–2199.
2. Schaller, R. D; Petruska, M. A; Klimov, V. I. Tunable Near-Infrared Optical Gain and Amplified Spontaneous Emission Using PbSe Nanocrystals. *J. Phys. Chem. B* **2003**, *107*, 13765–13768.
3. Klimov, V. I; Ivanov, S. A; Nanda, J; Achermann, M; Bezel, I; McGuire, J. A; Piryatinski, A. Single-Exciton Optical Gain in Semiconductor Nanocrystals. *Nature* **2007**, *447*, 441–446.
4. Dahan, M; Levi, S; Luccardini, C; Rostaing, P; Riveau, B; Triller, A. Diffusion Dynamics of Glycine Receptors Revealed by Single-Quantum Dot Tracking. *Science* **2003**, *302*, 442.
5. Gorman, J; Hasko, D. G; Williams, D. A. Charge-Qubit Operation of an Isolated Double Quantum Dot. *Phys. Rev. Lett.* **2005**, *95*, 090502.
6. Coe, S; Woo, W. K; Bawendi, M; Bulovic, V. Electroluminescence from Single Monolayers of Nanocrystals in Molecular Organic Devices. *Nature* **2002**, *420*, 800.
7. Koleilat, G. I; Levina, L; Shukla, H; Myrskog, S. H; Hinds, S; Pattantyus-Abraham, A. G; Sargent, E. H. Efficient, Stable Infrared Photovoltaics Based on Solution-Cast Colloidal Quantum Dots. *ACS Nano* **2008**, *2*, 833–840.
8. Alivisatos, A. P. Semiconductor Clusters, Nanocrystals, and Quantum Dots. *Science* **1996**, *271*, 933–937.
9. Nozik, A. J. Spectroscopy and Hot Electron Relaxation Dynamics in Semiconductor Quantum Wells and Quantum Dots. *Annu. Rev. Phys. Chem.* **2001**, *52*, 193.
10. Schaller, R. D; Petruska, M. A; Klimov, V. I. Effect of Electronic Structure on Carrier Multiplication Efficiency: Comparative Study of PbSe and CdSe Nanocrystals. *Appl. Phys. Lett.* **2005**, *87*, 253102.
11. McGuire, J. A; Joo, J; Pietryga, J. M; Schaller, R. D; Klimov, V. I. New Aspects of Carrier Multiplication in Semiconductor Nanocrystals. *Acc. Chem. Res.* **2008**, *41*, 1810–1819.
12. Beard, M. C; Knutsen, K. P; Yu, P; Luther, J. M; Song, Q; Metzger, W. K; Ellingson, R. J; Nozik, A. J. Multiple Exciton Generation in Colloidal Silicon Nanocrystals. *Nano Lett.* **2007**, *7*, 2506–2512.
13. Schaller, R. D; Pietryga, J. M; Klimov, V. I. Carrier Multiplication in InAs Nanocrystal Quantum Dots with an Onset Defined by the Energy Conservation Limit. *Nano Lett.* **2007**, *7*, 3469–3476.
14. Sambur, J. B; Novet, T; Parkinson, B. A. Multiple Exciton Collection in a Sensitized Photovoltaic System. *Science* **2010**, *330*, 63–66.
15. Semonin, O. E; Luther, J. M; Choi, S; Chen, H.-Y; Gao, J; Nozik, A. J; Beard, M. C. Peak External Photocurrent Quantum Efficiency Exceeding 100% *via* Meg in a Quantum Dot Solar Cell. *Science* **2011**, *334*, 1530–1533.
16. Zimmerman, P. M; Zhang, Z; Musgrave, C. B. Singlet Fission in Pentacene through Multi-Exciton Quantum States. *Nature Chem.* **2010**, *2*, 648–652.
17. Scholes, G. D; Rumbles, G. Excitons in Nanoscale Systems. *Nature Mat.* **2006**, *5*, 683–696.
18. Guyot-Sionnest, P; Shim, M; Matranga, C; Hines, M. Intraband Relaxation in CdSe Quantum Dots. *Phys. Rev. B* **1999**, *60*, R2181.
19. Cooney, R. R; Sewall, S. L; Dias, E. A; Sagar, D. M; Anderson, K. E. H; Kambhampati, P. Unified Picture of Electron and Hole Relaxation Pathways in Semiconductor Quantum Dots. *Phys. Rev. B* **2007**, *75*, 245311–1−14.
20. Klimov, V. I. Optical Nonlinearities and Ultrafast Carrier. *J. Phys. Chem. B* **200**, *104*, 6112.
21. Klimov, V. I; Mikhailvsky, A. A; Xu, S, V; Hollingsworth, J. A; Leatherdale, C. A; Eisler, M.-J; Bawendi, M. G. Optical Gain and Stimulated Emission in Nanocrystal Quantum Dots. *Science* **2000**, *290*, 314–317.
22. Harbold, J. M; Du, H; Krauss, T. D; Cho, K.-S; Murray, C. B; Wise, F. W. Time-Resolved Intraband Relaxation of Strongly Confined Electrons and Holes in Colloidal PbSe Nanocrystals. *Phys. Rev. B* **2005**, *72*, 195312.
23. Cooney, R. R; Sewall, S. L; Anderson, K. E. H; Dias, E. A; Kambhampati, P. Breaking the Phonon Bottleneck for Holes in Semiconductor Quantum Dots. *Phys. Rev. Lett.* **2007**, *98*, 177403.
24. Efros, A. L; Kharchenko, V. A; Rosen, M. Breaking the Phonon Bottleneck in Nanometer Quantum Dots − Role of Auger-Like Processes. *Solid State Commun.* **1995**, *93*, 281–284.
25. Klimov, V. I; Mikhailovsky, A. A; McBranch, D. W; Leatherdale, C. A; Bawendi, M. G. Mechanisms for Intraband Energy Relaxation in Semiconductor Quantum Dots: the Role of Electron-Hole Interactions. *Phys. Rev. B* **2000**, *61*, R13349.
26. Hendry, E; Koeberg, M; Wang, F; Zhang, H; Donega, C. D; Vanmaekelbergh, D; Bonn, M. Direct Observation of Electron-to-Hole Energy Transfer in CdSe Quantum Dots. *Phys. Rev. Lett.* **2006**, *96*, 057408.
27. Guyot-Sionnest, P; Wehrenberg, B; Yu, D. Intraband Relaxation in CdSe Nanocrystals and the Strong Influence of the Surface Ligands. *J. Chem. Phys.* **2005**, *123*, 074709.
28. Pandey, A; Guyot-Sionnest, P. Slow Electron Cooling in Colloidal Quantum Dots. *Science* **2008**, *322*, 929–932.
29. Chen, Y; Vela, J; Htoon, H; Casson, J. L; Werder, D. J; Bussian, D. A; Klimov, V. I; Hollingsworth, J. A. Giant Multishell CdSe Nanocrystal Quantum Dots with Suppressed Blinking. *J. Am. Chem. Soc.* **2008**, *130*, 5026–5027.
30. Garcia-Santamaria, F; Chen, Y; Vela, J; Schaller, R. D; Hollingsworth, J. A; Klimov, V. I. Suppressed Auger Recombination in Giant Nanocrystals Boosts Optical Gain Performance. *Nano Lett.* **2009**, *9*, 3482–3488.
31. Kambhampati, P. Unraveling the Structure and Dynamics of Excitons in Semiconductor Quantum Dots. *Acc. Chem. Res.* **2011**, *44*, 1–13.
32. Yurs, L. A; Block, S. B; Pakoulev, A. V; Selinsky, R. S; Jin, S; Wright, J. Multiresonant Coherent Multidimensional Electronic Spectroscopy of Colloidal PbSe Quantum Dots. *J. Phys. Chem. C* **2011**, *115*, 22833–22844.
33. Puzder, A; Williamson, A; Zaitseva, N; Galli, G; Manna, L; Alivisatos, A. The Effect of Organic Ligand Binding on the

Growth of CdSe Nanoparticles Probed by *Ab initio* Calculations. *Nano Lett.* **2004**, *4*, 2361–2365.
34. Puzder, A; Williamson, A. J; Gygi, F; Galli, G. Self-Healing of CdSe Nanoctystals: First-Principles Calculations. *Phys. Rev. Lett.* **2004**, *92*, 217401.
35. Yang, P; Tretiak, S; Masunov, A; Ivanov, S. Quantum Chemistry of the Minimal CdSe Clusters. *J. Chem. Phys.* **2008**, *129*, 074709.
36. Rempel, J. Y; Trout, B. L; Bawendi, M. G; Jensen, K. F. Density Functional Theory Study of Ligand Binding on CdSe (0001), (000$\bar{1}$), and (11$\bar{2}$0) Single Crystal Relaxed and Reconstructed Surfaces: Implications for Nanocrystalline Growth. *J. Phys. Chem. B* **2006**, *110*, 18007–18016.
37. Frenzel, J; Joswig, J.-O; Sarkar, P; Seifert, G; Springborg, M. The Effects of Organisation, Embedding and Surfactants on the Properties of Cadmium Chalcogenide (CdS, CdSe and CdS/CdSe) Semiconductor Nanoparticles. *Eur. J. Inorg. Chem.* **2005**, 3585–3596.
38. Yu, M; Fernando, G; Li, R; Papadimitrakopoulos, F; Shi, N; Ramprasad, R. First Principles Study of CdSe Quantum Dots: Stability, Surface Unsaturations, and Experimental Validation. *Appl. Phys. Lett.* **2006**, *88*, 231910.
39. Muljarov, E. A; Takagahara, T; Zimmermann, R. Phonon-Induced Exciton Dephasing in Quantum Dot Molecules. *Phys. Rev. Lett.* **2005**, *95*, 177405.
40. Kamisaka, H; Kilina, S. V; Yamashita, K; Prezhdo, O. V. Ultrafast Vibrationally-Induced Dephasing of Electronic Excitations in PbSe Quantum Dots. *Nano Lett.* **2006**, *6*, 2295–2300.
41. Kilina, S; Ivanov, S; Tretiak, S. Effect of Surface Ligands on Optical and Electronic Spectra of Semiconductor Nanoclusters. *J. Am. Chem. Soc.* **2009**, *131*, 7717–7726.
42. Semenov, Y. G; Kim, K. W. Phonon-Mediated Electron-Spin Phase Diffusion in a Quantum Dot. *Phys. Rev. Lett.* **2004**, *92*, 026601.
43. Isborn, C. M; Kilina, S. V; Li, X; Prezhdo, O. V. Generation of Multiple Excitons in PbSe and CdSe Quantum Dots by Direct Photoexcitation: First-Principles Calculations on Small PbSe and CdSe Clusters. *J. Phys. Chem. C* **2008**, *112*, 18291–18294.
44. Kamisaka, H; Kilina, S. V; Yamashita, K; Prezhdo, O. V. Ab initio Study of Temperature and Pressure Dependence of Energy and Phonon-Induced Dephasing of Electronic Excitations in CdSe and PbSe Quantum Dots. *J. Phys. Chem. C* **2008**, *112*, 7800–7808.
45. Reboredo, F. A; Zunger, A. Surface-Passivation-Induced Optical Changes in Ge Quantum Dots. *Phys. Rev. B* **2001**, *63*, 235314–235317.
46. Fischer, S. A; Crotty, A. M; Kilina, S. V; Ivanov, S. A; Tretiak, S. Passivating Ligand and Solvent Contributions to the Electronic Properties of Semiconductor Nanocrystals. *Nanoscale* **2012**, *4*, 904–914.
47. Albert, V; Ivanov, S; Tretiak, S; Kilina, S. Electronic Structure of Ligated CdSe Clusters: Dependence on DFT Methodology. *J. Phys. Chem. B* **2011**, *115*, 15793–15800.
48. Koposov, A. Y; Cardolaccia, T; Albert, V; Badaeva, E; Kilina, S; Meyer, T. J; Tretiak, S; Sykora, M. Formation of Assemblies Comprising Ru-Polypyridine Complexes and CdSe Nanocrystals Studied by ATR-FTR Spectroscopy and DFT Modeling. *Langmuir* **2011**, *27*, 8377–8383.
49. Kilina, S. V; Craig, C. F; Kilin, D. S; Prezhdo, O. V. Ab initio Time-Domain Study of Phonon-Assisted Relaxation of Charge Carriers in a PbSe Quantum Dot. *J. Phys. Chem. C* **2007**, *111*, 4871.
50. Kilina, S. V; Kilin, D. S; Prezhdo, O. V. Breaking the Phonon Bottleneck in PbSe and CdSe Quantum Dots: Time-Domain Density Functional Theory of Charge Carrier Relaxation. *ACS Nano* **2009**, *3*, 93–99.
51. Schaller, R. D; Pietryga, J. M; Goupalov, S. V; Petruska, M. A; Ivanov, S. A; Klimov, V. I. Breaking the Phonon Bottleneck in Semiconductor Nanocrystals *via* Multiphonon Emission Induced by Intrinsic Nonadiabatic Interactions. *Phys. Rev. Lett.* **2005**, *95*, 196401.
52. Califano, M; Zunger, A; Franceschetti, A. Efficient Inverse Auger Recombination at Threshold in CdSe Nanocrystals. *Nano Lett.* **2004**, *4*, 525.
53. Wang, L. W; Califano, M; Zunger, A; Franceschetti, A. Pseudopotential Theory of Auger Processes in CdSe Quantum Dots. *Phys. Rev. Lett.* **2003**, *91*, 056404.
54. Velizhanin, K. A; Piryatinski, A. Numerical Study of Carrier Multiplication Pathways in Nanocrystalline and Bulk Form of PbSe. *Phys. Rev. Lett.* **2011**, *106*, 207401.
55. Pijpers, J. J. H; Ulbricht, R; Tielrooij, K. J; Osherov, A; Golan, Y; Delerue, C; Allan, G; Bonn, M. Assessment of Carrier-Multiplication Efficiency in Bulk PbSe and PbS. *Nature Phys.* **2009**, *5*, 811.
56. Craig, C. F; Duncan, W. R; Prezhdo, O. V. Trajectory Surface Hopping in the Time-Dependent Kohn-Sham Approach for Electron-Nuclear Dynamics. *Phys. Rev. Lett.* **2005**, *95*, 163001.
57. Evans, C. M; Guo, L; Peterson, J. J; Maccagnano-Zacher, S; Krauss, T. D. Ultrabright PbSe Magic-Sized Clusters. *Nano Lett.* **2008**, *8*, 2896–2899.
58. Kasuya, A; Sivamohan, R; Barnakov, Y. A; Dmitruk, I. M; Nirasawa, T; Romanyuk, V. R; Kumar, V; Mamykin, S. V; Tohji, K; Jeyadevan, B; Shinoda, K; Kudo, T; Terasaki, O; Liu, Z; Belosludov, R. V; Sundararajan, V; Kawazoe, Y. Ultra-Stable Nanoparticles of CdSe Revealed from Mass Spectrometry. *Nature Mat.* **2004**, *3*, 99–102.
59. Winkler, U; Eich, D; Chen, Z. H; Fink, R; Kulkarni, S. K; Umbach, E. Detailed Investigation of CdS Nanoparticle Surfaces by High-Resolution Photoelectron Spectroscopy. *Chem. Phys. Lett.* **1999**, *306*, 95–102.
60. Sapra, S; Nanda, J; Pietryga, J. M; Hollingsworth, J. A; Sarma, D. D. Unraveling Internal Structures of Highly Luminescent PbSe Nanocrystallites Using Variable-Energy Synchrotron Radiation Photoelectron Spectroscopy. *J. Phys. Chem. B* **2006**, *110*, 15244–15250.
61. Kudera, S; Zanella, M; Giannini, C; Rizzo, A; Li, Y; Gigli, G; Cingolani, R; Ciccarella, G; Spahl, W; Parak, W. J; Manna, L. Sequential Growth of Magic-Size CdSe Nanocrystals. *Adv. Mater.* **2007**, *19*, 548–552.
62. Lin, Z; Franceschetti, A; Lusk, M. T. Size Dependence of the Multiple Exciton Generation Rate in CdSe Quantum Dots. *ACS Nano* **2010**, *5*, 2503.
63. Kilina, S. V; Kilin, D. S; Prezhdo, V. V; Prezhdo, O. V. Theoretical Study of Electron-Phonon Relaxation in PbSe and CdSe Quantum Dots: Evidence for Phonon Memory. *J. Phys. Chem. C* **2011**, *115*, 21641–21651.
64. Kresse, G; Furthmüller, J. Efficient Iterative Schemes for *Ab initio* Total-Energy Calculations Using a Plane-Wave Basis Set. *Phys. Rev. B* **1996**, *54*, 11169.
65. Perdew, J. P. (1991) *Electronic Structure of Solids*. (Akademie Verlag, Berlin).
66. Vanderbilt, D. Soft self-consistent pseudopotentials in a generalized eigenvalue formalism. *Phys. Rev. B* **19990**, *41*, 7892.
67. Tully, J. C. Molecular Dynamics with Electronic Transitions. *J. Chem. Phys.* **1990**, *93*, 1061.
68. Parahdekar, P. V; Tully, J. C. Mixed Quantum-Classical Equilibrium. *J. Chem. Phys.* **2005**, *122*, 094102.
69. Clark, J; Nelson, T; Tretiak, S; Cirmi, G; Lanzani, G. Femtosecond Torsional Relaxation. *Nature Phys.* **2012**, *8*, 225–231.
70. Nelson, T; Fernandez-Aberti, S; Chernyak, V; Roitberg, A. E; Tretiak, S. Nonadiabatic Excited-State Molecular Dynamics Modeling of Photoinduced Dynamics in Conjugated Molecules. *J. Phys. Chem. B* **2011**, *115*, 5402–5414.
71. Duncan, W. R; Prezhdo, O. V. Theoretical Studies of Photoinduced Electron Transfer in Dye-Sensitized TiO2. *Annu. Rev. Phys. Chem.* **2007**, *58*, 143–184.
72. Conwell, E. (1967) *High Field Transport in Semiconductors*. (Academic Press, New York).
73. Klein, M. C; Hache, F; Ricard, D; Flytzanis, C. Size Dependence of Electron-Phonon Coupling in Semiconductor Nanosphere: The Case of CdSe. *Phys. Rev. B* **1990**, *42*, 11123.